Magnetic anisotropy in low-dimensional ferromagnetic systems: Fe monolayers on Ag(001), Au(001), and Pd(001) substrates

Chun Li
Department of Physics and Astronomy, Northwestern University, Evanston, Illinois 60208-3112

A. J. Freeman
Department of Physics and Astronomy, Northwestern University, Evanston, Illinois 60208-3112
and
Materials Science Division, Argonne National Laboratory, Argonne, Illinois 60439-4843

H. J. F. Jansen
Department of Physics, Oregon State University, Corvallis, Oregon 97331-6507

C. L. Fu
Metals and Ceramics Division (Mail Stop MS-6114),
Oak Ridge National Laboratory, P.O. Box 2008, Oak Ridge, Tennessee 37831
(Received 13 April 1990)

A second-variation full-potential linear augmented-plane-wave total-energy method for thin-film ferromagnetic systems is used to study the spin-orbit-interaction contribution to the magnetic anisotropy. For a free-standing Fe monolayer, the spin magnetization is determined to lie in the plane. Results for Fe monolayers on Au(001), Ag(001), and Pd(001) substrates indicate a preference for the spin direction to be perpendicular to the plane of the film. Computational details for this magnetic anisotropy are also discussed.

I. INTRODUCTION

Magnetic transition metals on noble-metal substrates have been a focus in recent years of both experimental[1-10] and theoretical[11-15] studies of surface and interface magnetism. A large amount of work has been done on epitaxial Fe thin films on Ag, Au, and Pd because of the close match (less than 3%) of the lattice constants of these fcc substrates with bcc Fe(001). Of particular interest and importance is the magnetic anisotropy.

The advent of the surface and thin-film technology has made it possible for experimentalists to prepare well-characterized magnetic thin films. The magnetic-anisotropy properties of ferromagnetic thin films (Fe, Co, Ni, etc.) on various substrates have been studied via surface magneto-optic Kerr effect (SMOKE), ferromagnetic resonance (FMR), spin-polarized photoemission, etc. In ultrathin Fe(001) films on Ag(001) (less than 2.5 monolayers), the magnetization is found to lie along the surface normal.[3-5] Both in-plane[9] and perpendicular anisotropy[10] are observed for monolayer-range Fe(001) on Au(001). Liu *et al.*[10] reported a universal behavior of perpendicular spin orientation below a critical thickness of 6 monolayers or less in fcc Fe(100) on Cu(100), fcc Fe(111) on Ru(0001), bct Fe(100) on Pd(100), and bcc Fe(100) on Au(100).

The origin of magnetic anisotropy of 3*d* ferromagnetic materials was proposed by Van Vleck[16] more than 50 years ago to be the spin-orbit interaction. Still today, the theoretical understanding of the magnetic anisotropy in realistic systems remains a great challenge, because it is necessary to know in precise detail both the electronic structure and the total energy (the latter to $\pm 10^{-5}$ eV). First-principles magnetic-anisotropy calculations for bulk Fe, Ni, and Co have been reported by a few groups.[17-19] Pioneering calculations for the spin anisotropy of ferromagnetic monolayers of Fe, Ni, and V were carried out by Gay and Richter[20] using a self-consistent local-orbit (SCLO) approach. From these studies it became especially obvious that to obtain a realistic result for the anisotropy energy an accurate determination of the electronic structure is extremely important, and that the numerical details of the computational approach need to be treated carefully.

To study the magnetic anisotropy of metal surfaces and thin films, we developed a so-called "second-variation" method based on our highly precise total-energy full-potential linear augmented-plane-wave (FLAPW) approach, i.e., to solve the relativistic Dirac equation of the electronic system with a charge density obtained from a previous semirelativistic self-consistent calculation. By doing so, relativistic electronic wave functions are obtained, and the total energy of the system is solved as a function of the spatial orientation of the spin polarization, which yields the magnetic anisotropy.

However, the magnetic anisotropy so determined, i.e., the total-energy difference among various spin directions, is extremely sensitive to the convergence of the computa-

tional parameters, as well as to slight alterations of the physical environment of the magnetic atoms in the model calculation. First of all, the anisotropy energy arises primarily from the detailed electronic structure—especially the energy-band structures in regions near band crossings and the electron states close to the Fermi energy. Thus, a fine mesh of **k** points [$\sim$6000 **k** points in the two-dimensional Brillouin zone (2D BZ)] is essential for obtaining a realistic result. (By contrast $\sim$50 **k** points in an irreducible wedge of the 2D BZ were sufficient for obtaining a well-converged charge density from a semirelativistic calculation.) Furthermore, because of the nature of this fully relativistic calculation, in which the electronic wave functions are not eigenvectors of the spin operator, a larger set of LAPW basis functions is required for the convergence of the magnetic anisotropy energy.

In later sections of this paper, we present (i) the formalism and the computational approach to determining that part of the magnetic anisotropy originating from the spin-orbit interaction based on our FLAPW method, and (ii) computational results of magnetic anisotropy for a free-standing Fe monolayer, as well as for Fe monolayers on Ag(001), Au(001), and Pd(001) substrates. The computational conditions for this anisotropy are also discussed based on the electronic bands and Fermi surfaces.

II. FORMALISM AND METHODOLOGY

A. Spin-orbit interaction

The fully relativistic Kohn-Sham equation[21] of a single-particle wave function in an external magnetic field is

$$\left[\frac{c}{i}\underline{\boldsymbol{\alpha}}\cdot\nabla+(\underline{\beta}-\underline{\mathbb{1}}_4)mc^2-e\phi_{\text{eff}}(\mathbf{r})\underline{\mathbb{1}}_4+\mu_B\underline{\mathbb{1}}_4[\mathbf{B}_{\text{eff}}(\mathbf{r})-\mathbf{B}_{\text{xc}}(\mathbf{r})]\cdot\mathbf{L}+\mu_B\mathbf{B}_{\text{eff}}(\mathbf{r})\cdot\underline{\boldsymbol{\alpha}}\otimes\underline{\mathbb{1}}_2\right]\Psi(\mathbf{r})=\varepsilon\Psi(\mathbf{r})\ , \tag{1}$$

where (with units in which $\hbar=1$)

$$\mathbf{L}=\frac{\mathbf{r}\times\nabla}{i}\ , \tag{2}$$

$$\underline{\boldsymbol{\alpha}}=\begin{bmatrix}\underline{0}_{2\times2} & \boldsymbol{\sigma}\\ \boldsymbol{\sigma} & \underline{0}_{2\times2}\end{bmatrix},\quad \underline{\beta}=\begin{bmatrix}\underline{\mathbb{1}}_2 & \underline{0}_{2\times2}\\ \underline{0}_{2\times2} & -\underline{\mathbb{1}}_2\end{bmatrix}, \tag{3}$$

$$\phi_{\text{eff}}(\mathbf{r})=\phi_{\text{ext}}(\mathbf{r})+\phi_{\text{xc}}(\mathbf{r})+\int d^3r'\frac{\rho(\mathbf{r}')}{|\mathbf{r}-\mathbf{r}'|}\ , \tag{4}$$

$$\mathbf{B}_{\text{eff}}(\mathbf{r})=\mathbf{B}_{\text{ext}}(\mathbf{r})+\mathbf{B}_{\text{xc}}(\mathbf{r})+\frac{1}{c}\int d^3r'\frac{\mathbf{j}(\mathbf{r}')\times(\mathbf{r}-\mathbf{r}')}{|\mathbf{r}-\mathbf{r}'|^3}\ . \tag{5}$$

By ignoring the angular-momentum term in the Hamiltonian and the internal-current contribution of the effective magnetic field, we transform (1) into a matrix form:

$$\begin{bmatrix}\underline{V}(\mathbf{r}) & \frac{c}{i}\underline{\boldsymbol{\alpha}}\cdot\nabla\\ \frac{c}{i}\underline{\boldsymbol{\alpha}}\cdot\nabla & \underline{V}(\mathbf{r})-2mc^2\underline{\mathbb{1}}_2\end{bmatrix}\begin{bmatrix}\Phi\\ \chi\end{bmatrix}=\varepsilon\begin{bmatrix}\Phi\\ \chi\end{bmatrix}, \tag{6}$$

where Φ and χ are the large and small components of $\Psi(\mathbf{r})$, respectively, and

$$\underline{V}(\mathbf{r})=\phi_{\text{eff}}(\mathbf{r})\underline{\mathbb{1}}_2+\mu_B[\mathbf{B}_{\text{ext}}(\mathbf{r})+\mathbf{B}_{\text{xc}}(\mathbf{r})]\cdot\underline{\boldsymbol{\alpha}}\ . \tag{7}$$

By defining

$$f=2mc^2/(2mc^2+\varepsilon-V) \tag{8}$$

($\simeq1$, when $mc^2\gg\varepsilon-V$), we obtain the set of equations for Φ and χ:

$$\frac{1}{2m}\underline{\boldsymbol{\alpha}}\cdot\nabla(f\underline{\boldsymbol{\alpha}}\cdot\nabla\Phi)+(\varepsilon\underline{\mathbb{1}}_2-\underline{V})\Phi=\underline{0}_{2\times1} \tag{9}$$

and

$$\chi=-\frac{i}{2mc}\underline{\boldsymbol{\alpha}}\cdot f\nabla\Phi\ . \tag{10}$$

Taking into account the fact that

$$-\frac{1}{2m}\underline{\boldsymbol{\alpha}}\cdot\nabla(f\underline{\boldsymbol{\alpha}}\cdot\nabla\Phi)=\left[\frac{1}{2m}\nabla\cdot(f\nabla\Phi)+\frac{i\underline{\boldsymbol{\alpha}}}{2m}\cdot(\nabla f\times\nabla\Phi)\right], \tag{11}$$

TABLE I. Computational results using the semirelativistic FLAPW method for a free-standing Fe monolayer with the Ag(001) or Au(001) lattice constant. The muffin-tin (MT) radii used for Fe atoms are 2.2 a.u.

	Fe monolayer ($a=a_{\text{Ag}}=4.086$ Å)				Fe monolayer ($a=a_{\text{Au}}=4.078$ Å)			
MT charge:	s	p	d	Total	s	p	d	Total
Spin up	0.162	0.040	4.507	4.710	0.161	0.039	4.506	4.708
Spin down	0.131	0.034	1.419	1.584	0.130	0.033	1.435	1.598
Magnetic moment	$3.13\mu_B$				$3.11\mu_B$			
Fermi energy	4.40 eV				4.46 eV			

TABLE II. Computational parameters used in the second-variation procedure and magnetic-anisotropy energy ($E_{\text{perpendicular}} - E_{\text{in plane}}$) results for free-standing Fe monolayer at Ag or Au lattice constant.

	Fe monolayer (at $a_{Ag}=4.086$ Å)	Fe monolayer (at $a_{Au}=4.078$ Å)
MT radius (a.u.)	2.20	2.20
maximum l for angular momentum	10	10
Energy grid for DOS (Ry)	3.0×10^{-5}	3.0×10^{-5}
Number of **k** points in an irreducible wedge ($\frac{1}{8}$) of the first BZ	1250	800
Magnetic-anisotropy energy $E_{(\theta=0,\phi=0)}-E_{(\theta=\pi/2,\phi=0)}$ (eV/atom)	$+4.3\times10^{-5}$	$+3.3\times10^{-5}$

the relativistic Kohn-Sham Hamiltonian is then clearly the combination of the semirelativistic Hamiltonian and a spin-orbit-interaction term:

$$\underline{H}\begin{bmatrix}\Phi\\ \chi\end{bmatrix}=\underline{H}_{\text{semi}}\begin{bmatrix}\Phi\\ \chi\end{bmatrix}+\underline{H}_{\text{s.o.}}\begin{bmatrix}\Phi\\ \chi\end{bmatrix}, \tag{12}$$

where

$$\underline{H}_{\text{semi}}\begin{bmatrix}\Phi\\ \chi\end{bmatrix}=\begin{bmatrix}\underline{V}\Phi-(1/2m)\nabla\cdot(f\nabla\Phi)\\ -(i/2mc)\underline{\sigma}\cdot f\nabla\Phi\end{bmatrix} \tag{13}$$

and

$$\underline{H}_{\text{s.o.}}\begin{bmatrix}\Phi\\ \chi\end{bmatrix}=\begin{bmatrix}-(i\underline{\sigma}/2m)\cdot(\nabla f\times\nabla\Phi)\\ \underline{0}_{2\times1}\end{bmatrix}. \tag{14}$$

Denote the eigenfunctions of the semirelativistic Hamiltonian

$$\underline{H}_{\text{semi}}|n\rangle=\underline{H}_{\text{semi}}\begin{bmatrix}\Phi_n\\ \chi_n\end{bmatrix}=\varepsilon_n\begin{bmatrix}\Phi_n\\ \chi_n\end{bmatrix}. \tag{15}$$

Thus, the matrix elements of the relativistic Hamiltonian can be expressed in the set of basis functions consisting of the semirelativistic eigenfunctions:

$$\langle m|\underline{H}|n\rangle=\langle m|\underline{H}_{\text{semi}}|n\rangle+\langle m|\underline{H}_{\text{s.o.}}|n\rangle, \tag{16}$$

or

$$\underline{H}_{mn}=\varepsilon_n\delta_{mn}+(\underline{H}_{\text{s.o.}})_{mn}. \tag{17}$$

In local-spin-density (LSD) theory, the exchange-correlation magnetic field $\mathbf{B}_{xc}$ has the same spatial orientation as the external field, i.e., $\mathbf{B}_{xc}\|\mathbf{B}_{ext}$. Thus, the semirelativistic Hamiltonian has the following behavior:

$$[\underline{H}_{\text{semi}},\mathbf{B}_{ext}\cdot\underline{\sigma}]=\underline{0}_{2\times2}. \tag{18}$$

The spin part of the wave function can be expressed as an eigenvector of the operator $\mathbf{B}_{ext}\cdot\underline{\sigma}$ (which allows the eigenfunctions of different spin directions to be solved independently). The semirelativistic Hamiltonian does not give rise to the magnetic anisotropy—$\underline{H}_{\text{semi}}$ is independent of the spatial direction of $\mathbf{B}_{ext}$ (or $\underline{\sigma}$).

The spin-orbit-interaction term of the relativistic Hamiltonian connects the spin orientation with the spatial parameters of the crystal lattice, which results in the dependence of the total energy of the electronic system on the spin direction—the magnetic anisotropy. However, it is important to note that the spin-orbit-interaction term is not the only origin of magnetic anisotropy. The two terms we ignored when introducing Eq. (6), namely the angular-momentum and the magnetic field from the internal current, also contribute to the magnetic anisotropy. However, because of the complex nature of these terms, their effect on magnetic anisotropy is not yet clearly understood, and their contributions to the magnetic anisotropy have been neglected in the present approach.

B. Computational approach: Second variation procedure

To estimate the magnetic anisotropy originating from the spin-orbit interaction, we introduce here a "second-

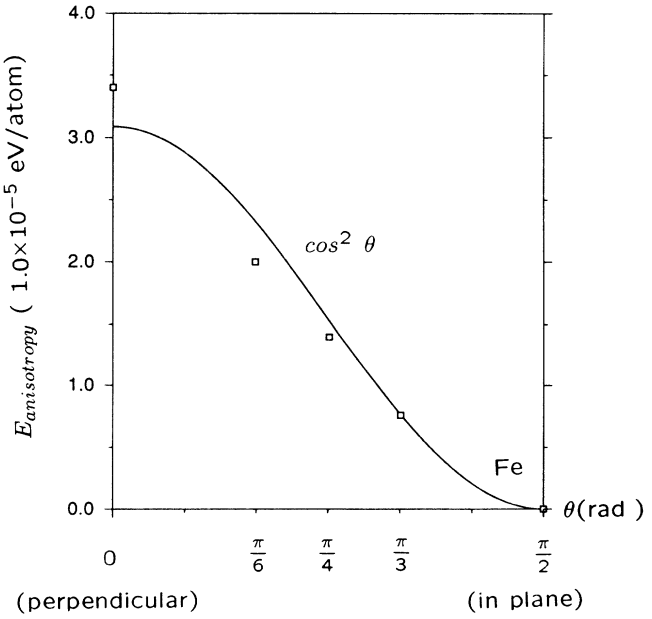

FIG. 1. Magnetic-anisotropy energy of a free-standing Fe(001) monolayer with Au lattice constant with respect to spin directions. The reference level is set so that $E(\theta=\pi/2,\phi=0)=0$. The solid line indicates the least-squares fitting of the $\cos^2(\theta)$ curve of the data points.

variation" procedure based on our full-potential linear augmented-plane-wave[22] method (FLAPW) for a two-dimensional periodic structure. Three steps are involved in this second-variation procedure: (i) again use the self-consistent FLAPW method to obtain the set of semirelativistic eigenfunctions described in Eq. (15), (ii) diagonalize the relativistic Hamiltonian with the variational method, and (iii) obtain the relativistic eigenvalues of the electronic states for various spin orientations in the real space:

$$H(\boldsymbol{\Sigma})\Psi_n(\mathbf{r})=\varepsilon_n(\boldsymbol{\Sigma})\Psi_n(\mathbf{r}) , \tag{19}$$

where $\boldsymbol{\Sigma}$ is the spatial orientation of the spin operator.

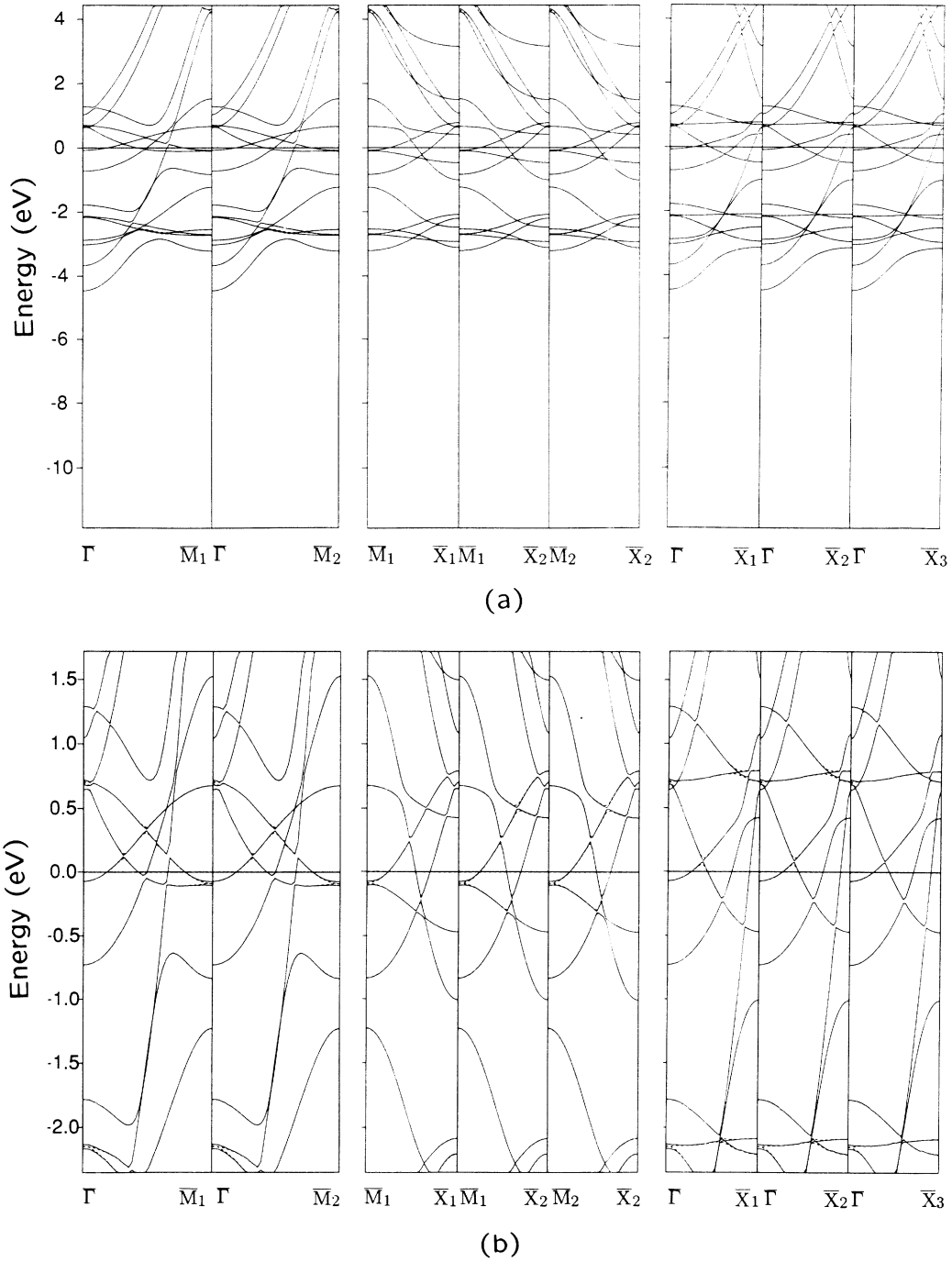

FIG. 2. Electronic band structure of a free-standing Fe(001) monolayer with Au lattice constant from the second-variation FLAPW method when spin-orbit interaction is taken into account. (a) All valence bands, and (b) states close to the Fermi level. Solid lines and dotted lines represent the ($\theta=0$, $\phi=0$) and ($\theta=\pi/2$, $\phi=0$) spin directions, respectively; (c) notation for the **k** directions used in (a) and (b) for the two-dimensional BZ.

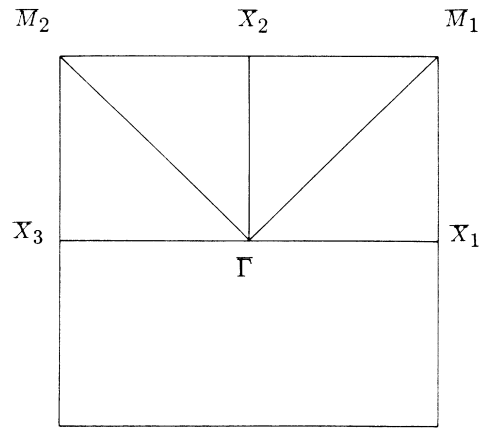

(c)

FIG. 2. (*Continued*).

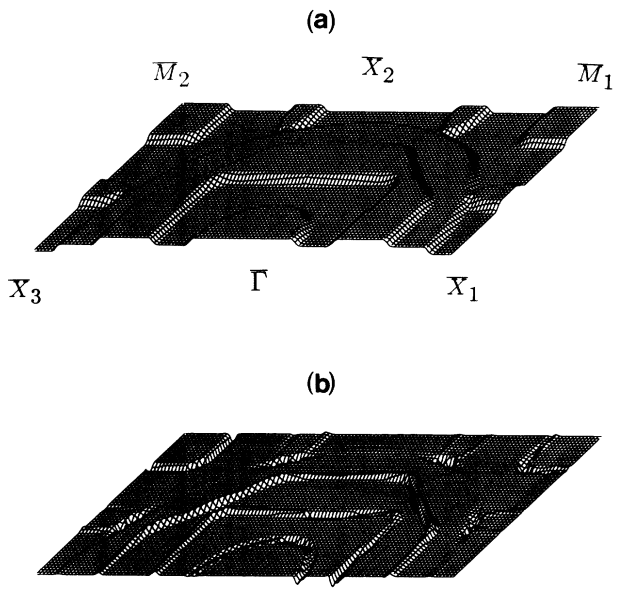

FIG. 3. **k**-space analysis of magnetic anisotropy for Fe monolayer at Au lattice constant. (a) Density of states (DOS) as a function of $\mathbf{k}-\Delta(\mathbf{k})=\int_{-\infty}^{\mu_F} D(\varepsilon,\mathbf{k})d\varepsilon$, plotted in the first BZ. (b) Magnetic anisotropy as a function of $\mathbf{k}-\Delta E(\mathbf{k})=\int_{-\infty}^{\mu_F(\Sigma_1)}\varepsilon D(\varepsilon,\mathbf{k},\Sigma_1)d\varepsilon-\int_{-\infty}^{\mu_F(\Sigma_2)}\varepsilon D(\varepsilon,\mathbf{k},\Sigma_2)d\varepsilon$, where $\Sigma_1=(\theta=0,\phi=0)$, $\Sigma_2=(\theta=\pi/2,\phi=0)$, plotted in the first BZ.

The magnetic anisotropy energy is estimated as

$$\Delta E=E(\Sigma_1)-E(\Sigma_2) \tag{20}$$

$$=\sum_{\text{occ. states}}\varepsilon_n(\Sigma_1)-\sum_{\text{occ. states}}\varepsilon_n(\Sigma_2) \tag{21}$$

$$=\int_{-\infty}^{\mu_F(\Sigma_1)}\varepsilon D(\varepsilon,\Sigma_1)d\varepsilon-\int_{-\infty}^{\mu_F(\Sigma_2)}\varepsilon D(\varepsilon,\Sigma_2)d\varepsilon\ , \tag{22}$$

where $\mu_F(\Sigma)$ is the Fermi energy of the electronic system and $D(\varepsilon,\Sigma)$ is the electronic density of states (DOS).

The FLAPW method is a local-spin-density[23] (LSD) -based computational method used to calculate the electronic structure and total energy of the electronic system in a periodic lattice. In this method there is no shape approximation made for either the charge density or the potential; all electrons are involved in the self-consistent process; the core electrons are treated fully relativistically and the valence electrons are treated semirelativistically. The exchange-correlation potential is calculated with use of the von Barth–Hedin[24] form. In the calculations, lattice harmonics with angular momenta up to $l=8$ are employed to expand the charge density and potential and to construct wave functions inside the muffin-tin (MT) spheres. To obtain the self-consistent semirelativistic charge density of the electronic system, 55 uniformly distributed **k** points in an irreducible wedge ($\frac{1}{8}$) of the 2D BZ are used.

In the second-variation calculations for the magnetic anisotropy the spin-orbit interaction is not treated self-consistently. As stated, the magnetic anisotropy is estimated as the difference in the eigenvalues of the occupied electronic states with respect to the spatial orientations of the electron spin from a second-variation approach. These magnetic-anisotropy energies have an extremely small value ($\sim 10^{-5}$ eV), and so demand a very careful numerical treatment to rule out the uncertainty resulting from computational errors. In the second-variation calculations we use identical computational parameters when solving the eigenvalues of the fully relativistic Hamiltonian with respect to different spatial spin orientations. When constructing matrix elements of the spin-orbit term of the Hamiltonian, we include all the occupied valence-electron states, as well as about 10 unoccupied states above the Fermi level. A very fine mesh of **k** points in the first BZ—equivalent to ~ 800 **k** points in the irreducible wedge of the 2D BZ for a semirelativistic calculation—is used to determine the total DOS, from which the Fermi energy and the sum of eigenvalues of the occupied states are calculated. In a later section we discuss the reason for requiring such a fine **k** mesh when calculating the magnetic anisotropy.

In this process we ignored the change of charge densities resulting from the spin-orbit interaction. However, considering the fact that the change in the total energy induced by the spin-orbit interaction is only $<10^{-5}$ eV/atom, we can reasonably assume that the effect on charge densities is also extremely small—very likely smaller than the error caused by computational uncertainties.

III. RESULTS AND DISCUSSIONS

A. Free-standing Fe monolayer

As the first test of our second-variation FLAPW method for calculating magnetic anisotropy, we studied the free-standing Fe monolayer with a square lattice structure and with lattice constants matching either fcc

Ag(001) (with $a_{Ag}=4.086$ Å) or fcc Au(001) (with $a_{Au}=4.078$ Å).

The charge density of the monolayer Fe is determined with use of the semirelativistic FLAPW method. Listed in Table I are the calculated charge populations of both spin directions inside the Fe MT sphere. The magnetic moment is determined by the difference of the majority- and minority-spin electron populations. As usual, the calculated magnetic moment ($\sim 3.1\mu_B$) for both lattice constants is strongly enhanced (by $\sim 41\%$) from the bulk value ($\sim 2.2\mu_B$). This enhancement results from the reduced bandwidth caused by the smaller number of neighboring atoms in the Fe monolayer compared with the bulk case. Only slight differences are seen between the electronic structure of these monolayer Fe films with different lattice constants.

The magnetic-anisotropy energy is estimated by the second-variation procedure. Note, however, that the results of this anisotropy energy are rather sensitive to a few computational parameters: (i) the maximum l value of the angular momentum used to express the charge density, potential, and wave functions (an $l=8$ expansion proves to be sufficient for obtaining convergence of the anisotropy energy); (ii) the energy window size used when obtaining semirelativistic wave functions which serve as basis for the fully relativistic eigenvalue problem (it is clear that all the occupied states and about 10 unoccupied states above the Fermi energy are needed; these include all Fe $3d$ states and the s-p states close to the Fermi energy); (iii) the energy grid when calculating the DOS of the system; (iv) the number of **k** points used to set up the **k** mesh in the first BZ (about 6000 **k** points in the first BZ are needed for proper convergence of the magnetic-anisotropy energy); and (v) the maximum magnitude of reciprocal-lattice vector (G_{max}) for plane-wave basis-function expansion—$G_{max}=3.5$ is sufficient to reach convergence for anisotropy calculations in the test case. The computational parameters used in the second-variation process and the magnetic-anisotropy energy for the free-standing Fe monolayers at Ag or Au lattice constants are listed in Table II.

In both systems a small in-plane reference of the spin orientation of order $\sim 3\times 10^{-5}$ eV/atom (or an equivalent anisotropy magnetic field of ~ 1.7 kG along the in-plane direction) is obtained from our calculations. We also calculated the anisotropy between the two in-plane directions, namely ($\theta=\pi/2, \phi=0$) and ($\theta=\pi/2, \phi=\pi/4$). This in-plane anisotropy energy is found to be about 2 orders of magnitude smaller than the perpendicular in-plane anisotropy, i.e., about 1% of the anisotropy energy between the ($\theta=0, \phi=0$) and ($\theta=\pi/2, \phi=0$) directions. Plotted in Fig. 1 is the anisotropy energy with respect to spin directions, $\theta=0$, $\pi/6$, $\pi/4$, $\pi/3$, and $\pi/2$. As expected, the anisotropy shows a $\cos^2\theta$-type curve.

Shown in Fig. 2 is the electronic band structure of a free-standing Fe monolayer at the Au(001) lattice constant with spin-orbit interaction taken into account. The solid and dashed lines represent the spin directions ($\theta=0, \phi=0$) and ($\theta=\pi/2, \phi=0$), respectively. The majority-spin electron bands are located from -3.7 to

TABLE III. Calculated results for monolayer Fe on Ag(001), Au(001), and Pd(001) substrates, and some computational parameters used when determining magnetic-anisotropy (MA) energy, ΔE_{MA} (in eV/atom), magnetic moments (in μ_B), and energy grid, $\Delta\varepsilon$ (in Ry).

	Fe/Au				Fe/Ag				Fe/Pd			
Fe charge:	s	p	d	Total	s	p	d	Total	s	p	d	Total
Spin up	0.14	0.09	4.46	4.69	0.15	0.08	4.44	4.67	0.16	0.10	4.45	4.72
Spin down	0.12	0.08	1.50	1.71	0.12	0.07	1.50	1.71	0.14	0.09	1.47	1.71
Moment/μ_B				2.98				2.96				3.01
Substrate:	Au				Ag				Pd			
Spin up	0.20	0.08	3.99	4.27	0.14	0.06	4.32	4.52	0.12	0.07	4.00	4.19
Spin down	0.21	0.07	3.90	4.19	0.15	0.07	4.26	4.49	0.12	0.07	3.65	3.85
Moment/μ_B				0.08				0.03				0.34
E_F	4.68 eV				4.63 eV				4.67 eV			
$\Delta\varepsilon$	4×10^{-5} Ry				3×10^{-5} Ry				3.15×10^{-5} Ry			
ΔE_{MA} [a]	-5.7×10^{-4}				-0.64×10^{-4}				-3.5×10^{-4}			

[a] $\Delta E_{MA}=E_{(\theta=0,\phi=0)}-E_{(\theta=\pi/2,\phi=0)}$, i.e., the energy difference between the perpendicular and in-plane directions.

-1.7 eV below the Fermi energy, and all five $3d$ states and one $4s$ state are fully occupied. The effect of the spin-orbit interaction is seen to be relatively larger at band crossings or for bands which are degenerate in the semirelativistic solution. The five $3d$ minority-spin states are located from -0.8 eV below E_F to $+1.2$ eV above E_F, and are only partially filled. Thus, the electron states close to the Fermi level are primarily those of minority spin. Shown in Fig. 3(a) is the **k**-space analysis of the density of states,

$$D(\mathbf{k})=\int_{-\infty}^{\mu_F} D(\varepsilon,\mathbf{k},\mathbf{\Sigma})d\varepsilon \ , \tag{23}$$

where $\mathbf{\Sigma}=(\theta=0,\phi=0)$. Sharp steps indicate the position of the Fermi surface. Figure 3(b) is the **k**-space analysis of the magnetic anisotropy,

$$\Delta E(\mathbf{k})=\int_{-\infty}^{\mu_F(\mathbf{\Sigma}_1)} D(\varepsilon,\mathbf{k},\mathbf{\Sigma}_1)d\varepsilon-\int_{-\infty}^{\mu_F(\mathbf{\Sigma}_2)} D(\varepsilon,\mathbf{k},\mathbf{\Sigma}_2)d\varepsilon \ , \tag{24}$$

where

$$\mathbf{\Sigma}_1=(\theta=0,\phi=0),\quad \mathbf{\Sigma}_2=(\theta=\pi/2,\phi=0) \ . \tag{25}$$

The magnetic-anisotropy energy arises from differences in the Fermi surfaces, as well as alterations of the energy levels of the electron states in the band structure. However, an analysis of the contribution to the magnetic anisotropy from different regions of **k** space in the first BZ shows that $\sim 45\%$ is from an area close to the Fermi surface, while $\sim 55\%$ is from the rest.

The resulting magnetic anisotropy is sensitive to the computational details, simply because of the precision required to determine such small values of their energies quantitatively. It is clear that among all the computational uncertainties, the error arising from the determination of the Fermi surface is the most critical factor. Thus, a very fine mesh of **k** points is needed to characterize the first BZ in reciprocal space. Moreover, a careful calculation for DOS of the electronic system is also important.

In contrast with the results of Gay and Richter,[20] but in agreement with the work of Karas *et al.*,[25] who also used the FLAPW approach, we find that the spin moment resides in the plane for Fe lattice constants chosen to match those of Ag and Au. (Since our calculated anisotropy-energy value is 4.3×10^{-5} and 3.3×10^{-5} eV, respectively, and the value of Gay and Richter is 10 times larger and that of Karas *et al.* is 100 times larger, the sensitivity to details of the differing computational schemes is apparent.)

B. Magnetic anisotropy of Fe monolayers on Au(001), Ag(001), and Pd(001) surfaces

For these theoretical studies, the Fe-metal systems are modeled by a single-slab geometry with one layer of $p(1\times1)$ Fe coupled with one layer of Ag (or Au or Pd) atoms, and the Fe atoms are located at the fourfold-hollow site of the Ag (or Au or Pd) square lattice. The experimental Ag, Au, and Pd lattice constants are assumed. The charge and magnetic moments are listed in Table III. In all three systems the calculated magnetic moments of the monolayer Fe atom, i.e., $2.96\mu_B$ in Fe/Ag, $2.98\mu_B$ in Fe/Au, and $3.01\mu_B$ in Fe/Pd, are remarkably close to that of the free Fe(001) surface value of $2.98\mu_B$, and close in value to those obtained from the previous calculations with the Ag (Ref. 12) or Au (Ref. 13) substrates represented by five-layer single slabs. Not surprisingly, the Fe magnetic moment for 1Fe/1Pd ($3.01\mu_B$) is somewhat smaller than the reference calculations ($3.19\mu_B$) of Blügel *et al.*,[15] who used seven layers of Pd. Thus, the magnetic properties of the monolayer Fe atoms on Ag(001) and Au(001) substrates appear to be well presented by the 1Fe/1Ag (or 1Au) model FLAPW calculations, while the 1Fe/1Pd remains somewhat uncertain.

The magnetic moments induced in the noble-metal substrates, i.e., $0.03\mu_B$ in 1Fe/Ag, $0.08\mu_B$ in 1Fe/1Au, and $0.34\mu_B$ in 1Fe/1Pd, demonstrate the varying influence of the Fe magnetic moment and are consistent with previous, thicker-film FLAPW calculations. The Pd substrate atoms have a magnetic moment about 1 order of magnitude larger than do Ag or Au in the interface, indicating a much stronger magnetic interaction between the Fe $3d$ and Pd $4d$ band electrons. We will find that this is also reflected in the spin- (magnetic-) anisotropy results obtained using the second-variation FLAPW method. The results and computational parameters used are listed in Table III.

The computational results can be summarized as (1) in all three systems, i.e., 1Fe/1Au, 1Fe/1Ag, and 1Fe/1Pd, the easy direction of the spin orientation of the spin orientation is perpendicular to the surface of the film, in

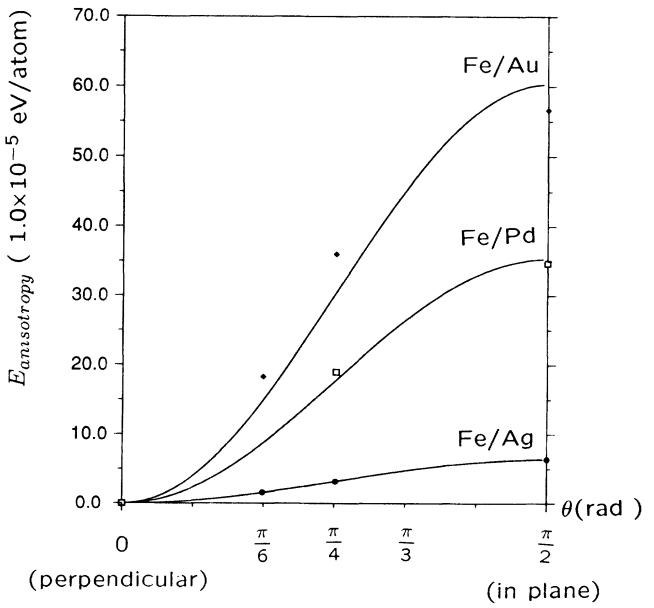

FIG. 4. Magnetic-anisotropy energy of (a) 1Fe/1Au, (b) 1Fe/1Ag, and (c) 1Fe/1Pd thin films with respect to spin directions; the reference level is set so that $E(\theta=0,\phi=0)=0$ [lines indicate the least-squares fitting of the $\sin^2(\theta)$ curves of the data points].

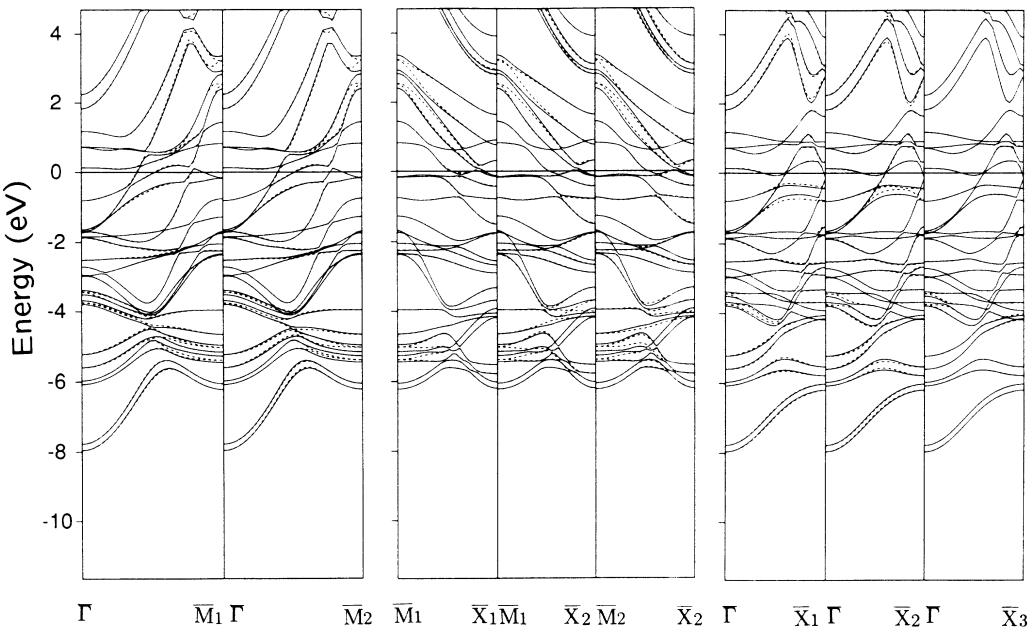

FIG. 5. Electronic band structure of a 1Fe/1Au(001) thin film with spin-orbit interaction taken into account. Solid lines and dotted lines represent the ($\theta=0$, $\phi=0$) and ($\theta=\pi/2$, $\phi=0$) spin directions, respectively.

contrast with our results for the free standing Fe(001) monolayer; (2) the values of the magnetic-anisotropy energy for these systems are considerably larger than our results from the free-standing Fe monolayer, i.e, 0.5 meV/atom for 1Fe/1Au, 0.1 meV/atom for 1Fe/1Ag, and 0.4 meV/atom for 1Fe/1Pd. In this case, the result for 1Fe/1Ag is in agreement with the preliminary result reported by Gay and Richter for an Fe/Ag(001) slab with five Ag layers sandwiched between a monolayer of Fe on either side. (See Fig. 4.)

Shown in Fig. 5 is the electronic band structure of 1Fe/1Au when the spin-orbit interaction is taken into account. The solid and dashed lines represent the spin directions ($\theta=0$, $\phi=0$) and ($\theta=\pi/2$, $\phi=0$), respectively. As expected, the spin-orbit-interaction correction for the states with a large weight at the Au atom is much larger than for those with large weight at an Fe atom. Because of the Fe-Au hybridization, the band structure at E_F is very different from that of the free-standing Fe monolayer. This difference is primarily responsible for the different magnetic anisotropy behavior of 1Fe/1Au (perpendicular) and a free-standing Fe monolayer (in plane).

By using 1 monolayer of Ag, Au, or Pd atoms to represent the noble-metal (001) substrate, these computational models are still far from being realistic in comparison to the experimentally used samples. However, considering the very short range of surface interface effects on noble-metal (001) structures,[26] it is expected that these results will yield some insight into the effect of the substrate on the magnetic-anisotropy energy of monolayer Fe(001) thin films. Because of the extremely computational-time-consuming nature of the calculations, we estimate that the current results still carry an uncertainty of at least ~40% based on experience obtained from detailed calculations on an Fe monolayer. We should thus consider these results to be qualitatively correct at this time.

These computational results, namely, perpendicular magnetic anisotropy of monolayer Fe on Au(001), Ag(001), or Pd(001), is consistent with experimental observations of the perpendicular orientations of Fe moments on Pd(001), Au(001), and Ag(001) by a few groups. The experimental determination of the magnitude of the magnetic anisotropy is available via FMR measurements. However, since the experimental values of the magnetic anisotropy range from 10^{-5} to 10^{-3} eV/atom for various Fe surface (thin-film) systems, the comparison of our calculated value with experiments is not significant at this time.

IV. CONCLUSIONS

The conclusion of this work is that the magnetic-anisotropy energy originating from the spin-orbit interactions, as obtained via use of a second-variation procedure, is in qualitatively agreement with the experimental results of monolayer-range Fe(001) thin films on Ag(001), Au(001), and Pd(001) substrates: all of these substrates show perpendicular orientation of the magnetization. By contrast, the free-standing Fe(001) monolayer model does not give the correct direction of the magnetic anisotropy of Fe thin films on these substrates. The magnetic-anisotropy energy depends on the details of the electronic structure of the system. We also propose that one layer of Ag, Au, and Pd is possibly sufficient to simulate the noble-metal substrate in the magnetic-anisotropy calculations. However, further studies of the magnetic anisotropy with a more realistic model, with second-variation or self-consistent procedures, of the thin films on these substrates are very important.

ACKNOWLEDGMENTS

We are grateful to Kristl Hathaway for stimulating discussions and encouragement, as well as to S. D. Bader and D. D. Koelling for helpful discussions. The work of Northwestern University was supported by the U.S. National Science Foundation (Grant No. DMR-88-16126, and by a grant of supercomputing time at the Pittsburgh Supercomputing Center) and the Office of Naval Research, U.S. Department of Defense (Grant No. N00014-89-J-1290). The work at Oregon State University was supported by the Office of Naval Research U.S. Department of Defense (Grant No. N00014-89-J-1165). The work at Oak Ridge National Laboratory was sponsored by the Division of Material Sciences of the Office of Basic Energy Sciences, U.S. Department of Energy, under Contract No. DE-AC05-85OR21400 with Martin Marietta Energy Systems, Inc. The work at Argonne National Laboratory was supported by the U.S. Department of Energy.

APPENDIX: SPIN-ORBIT OPERATOR IN SECOND-VARIATION FLAPW METHOD

We use the second-variation method to solve the fully relativistic eigenvalue problem by expressing the fully relativistic Hamiltonian in the basis of semirelativistic eigenfunctions. The spatial orientation of the spin system is taken into account by placing a zero-value external magnetic field $\mathbf{B}$ along the $(\cos\phi\sin\theta, \sin\phi\sin\theta, \cos\theta)$ directions. By doing so, the spin part of the semirelativistic eigenfunction can be determined as

$$\mathbf{B}\cdot\underline{\boldsymbol{\sigma}}\begin{bmatrix} a \\ b \end{bmatrix}_{\pm} = \pm|\mathbf{B}|\begin{bmatrix} a \\ b \end{bmatrix}_{\pm}, \tag{A1}$$

where

$$\mathbf{B}\cdot\underline{\boldsymbol{\sigma}} = \begin{bmatrix} B_z & B_x - iB_y \\ B_x + iB_y & -B_z \end{bmatrix}, \tag{A2}$$

and

$$|+\rangle = \begin{bmatrix} a \\ b \end{bmatrix}_{+} = \begin{bmatrix} \cos(\theta/2)e^{-i\phi/2} \\ \sin(\theta/2)e^{i\phi/2} \end{bmatrix}, \tag{A3}$$

$$|-\rangle = \begin{bmatrix} a \\ b \end{bmatrix}_{-} = \begin{bmatrix} \sin(\theta/2)e^{-i\phi/2} \\ -\cos(\theta/2)e^{i\phi/2} \end{bmatrix}. \tag{A4}$$

In spherical coordinates,

$$\nabla = \hat{\mathbf{r}}\nabla_r + \hat{\boldsymbol{\theta}}\nabla_\theta + \hat{\boldsymbol{\phi}}\nabla_\phi, \tag{A5}$$

and

$$l = -i\hat{\mathbf{r}}\times(\hat{\boldsymbol{\theta}}\nabla_\theta + \hat{\boldsymbol{\phi}}\nabla_\phi) \tag{A6}$$

is the angular-momentum operator.

Now, consider the spin-orbit term in the fully relativistic Hamiltonian equation (10):

$$-\frac{i\boldsymbol{\sigma}}{2m}\cdot(\nabla f\times\nabla)\Phi = -\frac{-i\boldsymbol{\sigma}}{2m}\frac{1}{[2mc+(\varepsilon-V)/c]^2}\cdot[\nabla_r V\cdot il\Phi - ilV\cdot\nabla_r\Phi + \hat{\mathbf{r}}(\nabla_\theta V\nabla_\phi\Phi - \nabla_\phi V\nabla_\theta\Phi)]. \tag{A7}$$

The first term in (A7) has the form of $\boldsymbol{\sigma}\cdot l\Phi$, and contributes the primary part of the spin-orbit interaction ($\sim$98% in the test case of a monolayer Fe film); hence, the other two terms are ignored in the calculation.

Thus, in our calculations, magnetic anisotropy arises from this $\underline{\boldsymbol{\sigma}}\cdot\boldsymbol{l}$ part, which can be transformed into

$$\frac{1}{[2m\varepsilon+(\varepsilon-V/c]^2}\frac{1}{r}\frac{\partial V}{\partial r}(\underline{\boldsymbol{\sigma}}\cdot\boldsymbol{l})\Phi. \tag{A8}$$

The four matrix elements of $\underline{\boldsymbol{\sigma}}\cdot\boldsymbol{l}$ are

$$\langle+|\underline{\boldsymbol{\sigma}}\cdot\boldsymbol{l}|+\rangle = \cos\theta\, l_z + \tfrac{1}{2}\sin\theta e^{-i\phi}l_+ + \tfrac{1}{2}\sin\theta e^{i\phi}l_-, \tag{A9}$$

$$\langle+|\underline{\boldsymbol{\sigma}}\cdot\boldsymbol{l}|-\rangle = \sin\theta\, l_z + \sin^2(\theta/2)e^{-i\phi}l_+ - \cos^2(\theta/2)e^{i\phi}l_-, \tag{A10}$$

$$\langle-|\underline{\boldsymbol{\sigma}}\cdot\boldsymbol{l}|+\rangle = (\langle+|\underline{\boldsymbol{\sigma}}\cdot\boldsymbol{l}|-\rangle)^{\dagger}, \tag{A11}$$

$$\langle-|\underline{\boldsymbol{\sigma}}\cdot\boldsymbol{l}|-\rangle = -\langle+|\underline{\boldsymbol{\sigma}}\cdot\boldsymbol{l}|+\rangle, \tag{A12}$$

where

$$l_\pm \equiv l_x \pm il_y. \tag{A13}$$

It is worth noting that the second-variation procedure does not give the "true" self-consistent solution of the fully relativistic Hamiltonian—even when we assumed that the charge density approximates the ground state, the direction of spin polarization does not necessarily represent the lowest energy. In principle, however, a self-consistent procedure will yield the ground-state solution of the fully relativistic Hamiltonian. The so-obtained ground state should be dependent on both the spatial direction and the value of the external magnetic field when spin-orbit interaction is present.

In the second-variation procedure presented in this work, the total energy of the electron system is obtained for a fixed spatial orientation of the spin polarization and a zero external magnetic field—the difference of so-determined total energies resembles the magnetic-anisotropy energy. Such a procedure is well grounded for the following reasons.

(i) The effect of the external magnetic field on the magnetic anisotropy can be ignored; this is fairly sound because the electronic structure is not affected by the external magnetic field when the majority-spin bands are fully filled, as is seen in monolayer Fe thin films.

(ii) We can thus assume that the fixed spatial orientation of spin polarization resembles the case in which the

spin is aligned by a strong external magnetic field. The isotropic magnetic energy, $\mathbf{B}\cdot\mathbf{M}$, does not contribute to the magnetic anisotropy, and thus can be replaced by a zero field here.

Finally, it goes without saying that a final judgment of the validity of this second-variation procedure relies on the self-consistent solution of the fully relativistic Hamiltonian.

[1]M. Stampanoni *et al.*, Phys. Rev. Lett. **59**, 2483 (1987).
[2]A. Vaterlaus *et al.*, J. Appl. Phys. **64**, 5331 (1988).
[3]B. Heinrich *et al.*, Phys. Rev. Lett. **59**, 1756 (1987).
[4]B. T. Jonker *et al.*, Phys. Rev. Lett. **57**, 142 (1986).
[5]N. C. Koon *et al.*, Phys. Rev. Lett. **59**, 2463 (1987).
[6]S. D. Bader, E. R. Moog, and R. Grunberg, J. Magn. Magn. Mater. **53**, 1295 (1986).
[7]S. D. Bader and E. R. Moog, J. Appl. Phys. **61**, 3729 (1987).
[8]S. T. Purcell, B. Heinrich, and A. S. Arrott, J. Appl. Phys. **64**, 5337 (1988).
[9]W. Dürr *et al.*, Phys. Rev. Lett. **62**, 206 (1989).
[10]C. Liu and S. D. Bader, J. Vac. Sci. Technol. A (to be published).
[11]S. Ohnishi, A. J. Freeman, and M. Weinert, Phys. Rev. B **18**, 6741 (1983).
[12]A. J. Freeman and C. L. Fu, J. Appl. Phys. **61**, 3356 (1987).
[13]Chun Li, A. J. Freeman, and C. L. Fu, J. Magn. Magn. Mater. **75**, 201 (1988).
[14]C. L. Fu, A. J. Freeman, and T. Oguchi, Phys. Rev. B **34**, 2700 (1985).
[15]S. Blügel, M. Weinert, and P. H. Dederichs, Phys. Rev. Lett. **60**, 1077 (1988).
[16]J. H. Van Vleck, Phys. Rev. **52**, 1178 (1937).
[17]L. Fritsche, J. Noffke, and H. Eckardt, J. Phys. F **17**, 943 (1987).
[18]G. H. Daalderop, P. J. Kelly, M. F. H. Schuurmans, and H. J. F. Jansen, J. Phys. (Paris) Colloq. **50**, C8-93 (1989).
[19]P. Strange, H. Ebert, J. B. Staunton, and B. L. Gyorffy, J. Phys. Condens. Matter **1**, 3947 (1989).
[20]J. G. Gay and R. Richter, Phys. Rev. Lett. **56**, 2728 (1986); J. Appl. Phys. **61**, 3362 (1987).
[21]H. J. F. Jansen, Phys. Rev. B **38**, 8022 (1988).
[22]E. Wimmer, A. J. Freeman, and H. Krakauer, Phys. Rev. B **30**, 3113 (1984).
[23]W. Kohn and L. Sham, Phys. Rev. **140**, A1133 (1965).
[24]V. von Barth and L. Hedin, J. Phys. C **5**, 1629 (1972).
[25]W. Karas, J. Noffke, and L. Fritsche, J. Phys. (Paris) Colloq. (to be published).
[26]H. Erschbaumer and A. J. Freeman (unpublished).